

Quantum-memory-assisted entropic uncertainty principle, teleportation and entanglement witness in structured reservoirs

Ming-Liang Hu^{1,*} and Heng Fan^{2,†}

¹*School of Science, Xi'an University of Posts and Telecommunications, Xi'an 710121, China*

²*Beijing National Laboratory for Condensed Matter Physics,
Institute of Physics, Chinese Academy of Sciences, Beijing 100190, China*

We relate the principle of quantum-memory-assisted entropic uncertainty to quantum teleportation and show geometrically that any two-qubit state which lowers the upper bound of this uncertainty relation is useful for teleportation. We also explore the efficiency of this entropic uncertainty principle on witnessing entanglement in a general class of bosonic structured reservoirs. The entanglement regions witnessed by different estimates are determined, which may have no relation with the explicit form of the spectral density of the reservoir for certain special chosen sets of the initial states.

PACS numbers: 03.67.Mn, 03.65.Ta, 03.65.Yz

I. INTRODUCTION

The uncertainty principle initially observed by Heisenberg [1] for the case of position and momentum, and further formulated by Robertson [2] for arbitrary pairs of observables is a central in quantum theory. It sets limits on our ability to predict the precise outcomes of two incompatible measurements on a quantum system, and at the same time provides the basis for new technologies such as quantum cryptography [3] in quantum information. Originally, the uncertainty relation is expressed in terms of the standard deviation $\Delta R \cdot \Delta S \geq \frac{1}{2} |\langle [R, S] \rangle|$ for two observables R and S [2]. However, this uncertainty bound is state-dependent and also trivial for finite-valued observables [4]. To remove this pitfall and to precisely capture its physical meanings, the original form has subsequently been recast to the entropic one [5], which reads

$$H(R) + H(S) \geq \log_2 \frac{1}{c}, \quad (1)$$

where $H(R)$ denotes the Shannon entropy of the probability distribution of the outcomes when R is measured, and likewise for $H(S)$. $1/c$ quantifies the complementarity of R and S , where $c = \max_{r,s} |\langle \Psi_r | \Phi_s \rangle|^2$ for nondegenerate observables, with $|\Psi_r\rangle$ and $|\Phi_s\rangle$ being the eigenvectors of R and S .

The above uncertainty limitation applies to the case that the observer can access only to the classical information. It may be violated through clever use of entanglement, which plays a central role in quantum information. This is the quantum-memory-assisted entropic uncertainty principle, which was previously conjectured by Renes and Boileau [6], and later being strictly proved by Berta *et al.* [7]. It states that if the observer can entangle the particle A that he wishes to measure with

another particle B which serves as a quantum memory, then the uncertainty of this observer about any pair of observables can be dramatically reduced. Particularly, if A and B are maximally entangled, then the observer is able to correctly predict the outcomes of whichever measurement is chosen. This new entropic uncertainty relation reads

$$H(R|B) + H(S|B) \geq \log_2 \frac{1}{c} + H(A|B), \quad (2)$$

where $H(R|B)$ is the conditional von Neumann entropy of the postmeasurement state $\rho_{RB} = \sum_r (|\Psi_r\rangle\langle\Psi_r| \otimes \mathbb{I}) \rho_{AB} (|\Psi_r\rangle\langle\Psi_r| \otimes \mathbb{I})$, and likewise for $H(S|B)$. Compared with Eq. (1), there is an extra term $H(A|B)$ (the conditional von Neumann entropy of ρ_{AB}) appearing on the right-hand side of Eq. (2). In particular, if $H(A|B)$ is negative, the Berta *et al.* bound (BB) of uncertainty in Eq. (2) can be reduced comparing with previous uncertainty relation. It is also found that this negative value gives the lower bound of the one-way distillable entanglement between A and B [8].

This new entropic uncertainty principle has been recently confirmed experimentally [4, 9], and ignites interests of people on investigating its potential applications from various aspects [10]. In this work, we will first relate it to quantum teleportation, and show that any two-qubit ρ_{AB} with negative $H(A|B)$ gives nonclassical teleportation fidelity. It is known that teleportation is one fundamental protocol in quantum information processing [11]. It is crucial, both theoretically and experimentally, to know whether the fidelity of teleportation is in classical regime or in quantum regime. Our result relate this important problem to the entropic uncertainty principle.

We will also investigate efficiency of this new entropic uncertainty relation on witnessing entanglement in a class of bosonic structured reservoirs. It is known that entanglement plays a key role in quantum information processing such as in teleportation and in condensed matter physics; see, for example, Refs. [12, 13]. The point of departure for this practical application (i.e., entanglement witness) is Eq. (2), from which one can note that

*Electronic address: mingliang0301@163.com

†Electronic address: hfan@iphy.ac.cn

if $H(R|B) + H(S|B) < \log_2(1/c)$, then $H(A|B) < 0$, and hence ρ_{AB} is entangled [8]. Experimentally, the value of $H(R|B) + H(S|B)$ can be estimated by conditional single-qubit tomography on B [4], and this estimate is termed tomographic estimate (TE).

There are other ways for estimating the uncertainty. The first is the measurement estimate (ME) denoted by $H(R|R) + H(S|S)$, which corresponds to the same measurements on both A and B , and are favored for its ease of implementation [4]. This estimate provides an upper bound for the new uncertainty relation in that quantum measurements never decrease entropy. The second is the Fano estimate (FE) obtained by using Fano's inequality $H(X|B) \leq h(p_X) + p_X \log_2(d-1)$ [14], where $h(p_X)$ is the binary entropy function, with p_X being the probability that the outcomes of X on A and X on B are different, and d is the dimension of A . For the two-qubit system (i.e., $d = 2$), the inequality $h(p_R) + h(p_S) < \log_2(1/c)$ is a signature of entanglement between A and B .

II. LINKING THE NEW ENTROPIC UNCERTAINTY RELATION TO TELEPORTATION

In this section we relate the quantum-memory-assisted entropic uncertainty principle to quantum teleportation. We will show that any two-qubit state with negative conditional von Neumann entropy, which thus lowers the upper bound of the uncertainty, is a manifestation of its usefulness for nonclassical teleportation.

Without loss of generality, we suppose the sender Alice wants to teleport to the receiver Bob a general one-qubit state, with a two-qubit state τ_{AB} (pure or mixed) being used as the quantum channel. Then if they adopt the standard teleportation scheme (i.e., Alice performs the Bell-basis measurement while Bob is equipped to perform any unitary transformation), the maximal average fidelity achievable can be evaluated as [15]

$$F_{\text{av}} = \frac{1}{2} + \frac{1}{6}N(\tau_{AB}), \quad (3)$$

where $N(\tau_{AB}) = \text{tr}\sqrt{T^\dagger T}$, with T being the 3×3 positive matrix with elements t_{ij} related to the Bloch sphere representation of τ_{AB} below

$$\tau_{AB} = \frac{1}{4}(\mathbb{I} \otimes \mathbb{I} + \vec{x} \cdot \vec{\sigma} \otimes \mathbb{I} + \mathbb{I} \otimes \vec{y} \cdot \vec{\sigma} + \sum_{i,j=1}^3 t_{ij} \sigma_i \otimes \sigma_j), \quad (4)$$

where \mathbb{I} is the 2×2 identity operator, $\vec{\sigma} = (\sigma_1, \sigma_2, \sigma_3)$ is the vector of the Pauli spin matrices, $\vec{x} = (x_1, x_2, x_3)$ and $\vec{y} = (y_1, y_2, y_3)$ are the local Bloch vectors in \mathbb{R}^3 with $\vec{x} \cdot \vec{\sigma} = \sum_{i=1}^3 x_i \sigma_i$ and $\vec{y} \cdot \vec{\sigma} = \sum_{i=1}^3 y_i \sigma_i$.

Since the teleportation fidelity is locally unitary invariant, and we can always find unitary operators \mathcal{U}_A and \mathcal{U}_B which transform the state τ_{AB} into

$$\rho_{AB} = \frac{1}{4}(\mathbb{I} \otimes \mathbb{I} + \vec{r} \cdot \vec{\sigma} \otimes \mathbb{I} + \mathbb{I} \otimes \vec{s} \cdot \vec{\sigma} + \sum_{k=1}^3 v_k \sigma_k \otimes \sigma_k), \quad (5)$$

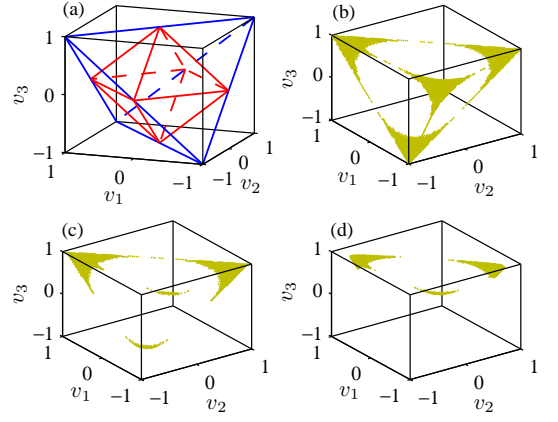


FIG. 1: (Color online) Geometry of the tetrahedron \mathcal{T} and the octahedron \mathcal{O} associated with the vector \vec{v} of ρ_{AB} (a), and valid regions of \vec{v} constrained by $H(A|B) < 0$ for $\vec{r} = \vec{s} = (0, 0, 0)$ (b), $(0, 0, 0.25)$ (c), and $(0.1, 0.1, 0.25)$ (d).

with $\vec{r} = (r_1, r_2, r_3)$ and $\vec{s} = (s_1, s_2, s_3)$, it suffices to restrict our concern to the representative class of quantum channels expressed in Eq. (5) with less number of parameters, for which we always have

$$N(\rho_{AB}) = \sum_{k=1}^3 |v_k|. \quad (6)$$

$N(\rho_{AB}) > 1$ gives $F_{\text{av}} > 2/3$ and thus ρ_{AB} is competent for teleportation.

The real numbers r_k , s_k , and v_k ($k = 1, 2, 3$) in Eq. (5) must satisfy certain constraints such that ρ_{AB} is a well defined density operator. Particularly, for the special case of $\vec{r} = \vec{s} = 0$, physical ρ_{AB} are those with (v_1, v_2, v_3) (for simplicity, we just refer to \vec{v} in the following) belongs to the tetrahedron \mathcal{T} (see Fig. 1) with vertices $(-1, 1, 1)$, $(1, -1, 1)$, $(1, 1, -1)$ and $(-1, -1, -1)$, among which separable ones are confined to the octahedron \mathcal{O} with vertices $(\pm 1, 0, 0)$, $(0, \pm 1, 0)$, and $(0, 0, \pm 1)$ [16]. The Bell states sit at the four vertices of \mathcal{T} , while the Werner states [17] are those represented by the lines connecting the vertices of \mathcal{T} with the origin of \mathcal{O} .

For the nonzero values of \vec{r} and/or \vec{s} , the vector \vec{v} which admits the positive semidefiniteness of ρ_{AB} also belongs to \mathcal{T} [16]. But now some \vec{v} inside \mathcal{T} may not correspond to the physical states. Moreover, while all the separable states are still confined to \mathcal{O} , there are also entangled ones with \vec{v} belongs to \mathcal{O} , which is different from the case of $\vec{r} = \vec{s} = 0$.

Since the octahedron \mathcal{O} is specified by $\sum_{k=1}^3 |v_k| \leq 1$, one can see from Eq. (6) that any physical ρ_{AB} with \vec{v} belongs to the four small tetrahedra divided by \mathcal{O} (i.e., the regions inside \mathcal{T} and outside \mathcal{O}) gives $N(\rho_{AB}) > 1$ and thus is useful for quantum teleportation. Physical ρ_{AB} confined to \mathcal{O} may also be entangled when the inner product $(\vec{r}, \vec{s}) \neq 0$, but they are useless for teleportation.

Now we begin to discuss the operational identification of ρ_{AB} useful for teleportation, and to what degree this

identification can cover the whole set of physical ρ_{AB} useful for teleportation. When considering the standard protocol, Horodecki *et al.* proved that any ρ_{AB} which violates the Bell-Clauser-Horne-Shimony-Holt (Bell-CHSH) inequality is useful for teleportation [15]. Here, we will show that the negativity of the conditional von Neumann entropy of ρ_{AB} is also a signature of its usefulness for teleportation. Particularly, these ρ_{AB} can be witnessed by means of the new entropic uncertainty relation, and therefore is expected to have potential applications in experiments.

To prove the above argument, we consider first ρ_{AB} associated with the vertices of \mathcal{O} . The positive semidefiniteness requires that the matrix elements $\rho_{AB}^{11}\rho_{AB}^{44} \geq |\rho_{AB}^{14}|^2$ and $\rho_{AB}^{22}\rho_{AB}^{33} \geq |\rho_{AB}^{23}|^2$, which yield $r_3 = s_3 = 0$ for physical states. For example, if $\vec{v} = (1, 0, 0)$ the above requirements turn to $1 - (r_3 + s_3)^2 \geq 1$ and $1 - (r_3 - s_3)^2 \geq 1$, which are satisfied only when $r_3 = s_3 = 0$.

Under the conditions of $r_3 = s_3 = 0$, we can write the explicit forms of ρ_{AB} at the vertices of \mathcal{O} , and further determine the constraints imposed on the parameters by positive semidefiniteness of ρ_{AB} . We use another property of the physical ρ_{AB} , which says that if a Hermitian matrix is positive semidefinite then all of its principal minors must be non-negative.

For ρ_{AB} with $\vec{v} = (1, 0, 0)$, we derive the second- and third-order leading principal minors as

$$D_2 = \frac{1 - s_1^2 - s_2^2}{16}, \quad D_3 = -\frac{(r_1 - s_1)^2 + (r_2 - s_2)^2}{64}. \quad (7)$$

We see that $s_1^2 + s_2^2 \leq 1$, $r_1 = s_1$ and $r_2 = s_2$ must be satisfied for ensuring the positive semidefiniteness of ρ_{AB} . Furthermore, the determinant of the (3,3) minor formed by removing from ρ_{AB} its third row and third column (i.e., one of the third-order principal minor) can be determined as $\Delta_3 = -r_2^2/16$, $\Delta_3 \geq 0$ further gives $r_2 = 0$. Then under the conditions of $r_{2,3} = s_{2,3} = 0$ and $-1 \leq r_1 = s_1 \leq 1$ we obtain the eigenvalues of ρ_{AB} as $\epsilon_{1,2} = 0$, $\epsilon_{3,4} = (1 \pm r_1)/2$, and the eigenvalues of the reduced $\rho_B = \text{tr}_A \rho_{AB}$ as $\epsilon_{1,2} = (1 \pm r_1)/2$. These give rise to the quantum conditional entropy $H(A|B) = 0$.

In fact, one can also determine $r_2 = 0$ by the argument that ρ_{AB} is positive semidefinite if $\text{tr}(\rho_{AB}\mathcal{P}) \geq 0$ for any projector \mathcal{P} . Taking $\mathcal{P} = uu^\dagger$ with $u = (u_1, u_2, u_3, u_4)^T$ and T denoting transpose, we obtain

$$\begin{aligned} \text{tr}(\rho_{AB}\mathcal{P}) = & \frac{1}{4}(|u_{14}^+|^2 + |u_{23}^+|^2) + \frac{1}{2}[r_1 \text{Re}(u_{14}^+ u_{23}^{+*}) \\ & - r_2 \text{Im}(u_{14}^- u_{23}^{+*})], \end{aligned} \quad (8)$$

where $u_{ij}^\pm = u_i \pm u_j$, with $\text{Re}(f)$ and $\text{Im}(f)$ representing the real and imaginary parts of f . One can check directly that only when $r_2 = 0$ can $\text{tr}(\rho_{AB}\mathcal{P}) \geq 0$ for any \mathcal{P} .

By using the same methodology we obtain constraints imposed on the parameters of ρ_{AB} associated with the remaining five vertices of \mathcal{O} , they are: $r_{1,3} = s_{1,3} = 0$ and $-1 \leq r_2 = \pm s_2 \leq 1$ for $\vec{v} = (0, \pm 1, 0)$, $r_{1,2,3} = s_{1,2,3} = 0$ for $\vec{v} = (0, 0, \pm 1)$, $r_{2,3} = s_{2,3} = 0$ and $-1 \leq r_1 = -s_1 \leq 1$

for $\vec{v} = (-1, 0, 0)$. All of these correspond to physical ρ_{AB} with $H(A|B) = 0$.

On the other hand, physical states ρ_{AB} with \vec{v} belonging to \mathcal{O} can always be written as a convex combination of states with \vec{v} at the vertices of \mathcal{O} , so by using the concavity of the quantum conditional entropy [14], we obtain $H(A|B) \geq 0$ for any density matrix ρ_{AB} belongs to \mathcal{O} [it is also possible for $H(A|B) \geq 0$ with ρ_{AB} lying beyond \mathcal{O}]. This means that for any physical ρ_{AB} with negative conditional entropy, \vec{v} must belong to the four tetrahedra separated by \mathcal{O} , which gives $\sum_{k=1}^3 |v_k| > 1$, and thus makes it useful for nonclassical teleportation.

We would like to point out here that the negativity of the conditional von Neumann entropy and the violation of the Bell-CHSH inequality [15] identify different subsets of density matrices useful for teleportation; namely, there are ρ_{AB} with $H(A|B) < 0$ but do not violate the Bell-CHSH inequality [e.g., ρ_{AB} of Eq. (5) with $\vec{r} = \vec{s} = (0, 0, 0.25)$ and $\vec{v} = (\pm 0.95, \mp 0.25, 0.30)$], while there are also ρ_{AB} which violate the Bell-CHSH inequality but with $H(A|B) > 0$ (e.g., the partial of the extended Werner-like states [17]).

In Fig. 1 we presented regions of the valid \vec{v} determined by $H(A|B) < 0$ with different \vec{r} and \vec{s} , from which one can see that for the Bell-diagonal states (i.e., $\vec{r} = \vec{s} = 0$), they locate near the four vertices of \mathcal{T} and are symmetric with respect to the origin of \mathcal{O} . For the general case ($\vec{r}, \vec{s} \neq 0$), however, the valid \vec{v} makes $H(A|B) < 0$ will shrink to small regions and their distribution are not symmetric with respect to the origin of \mathcal{O} .

The geometric characterization of ρ_{AB} also allows us to determine fractions of different kinds of ρ_{AB} over the ensemble of physical ρ_{AB} . This can be estimated by calculating ratio of volumes of the three-dimensional spaces occupied by \vec{v} associated with different ρ_{AB} . Here we obtained the corresponding volumes by performing Monte Carlo simulations, generating 10^9 random \vec{v} uniformly distributed in the cube illustrated in Fig. 1(a), and checking if they correspond to physical ρ_{AB} , if they give rise to $F_{av} > 2/3$ and if they make $H(A|B) < 0$. In this way we confirmed that 50% of the Bell-diagonal states ρ_{AB} give $F_{av} > 2/3$ (the volume of \mathcal{T} is twice that of \mathcal{O}), and about 4.17% of the Bell-diagonal ρ_{AB} make $H(A|B) < 0$. Therefore, about 8.34% of the Bell-diagonal ρ_{AB} useful for teleportation can be identified by negativity of the conditional entropy. Using the same method, we have also performed simulation for \vec{r} and \vec{s} chosen in Fig. 1(c) and 1(d), and confirmed that for the former (latter) case about 41.68% (35.51%) of the physical ρ_{AB} are useful for teleportation, among which about 6.16% (3.30%) of them have negative quantum conditional entropy.

III. ENTANGLEMENT WITNESS IN STRUCTURED RESERVOIRS

Entanglement is a precious resource for quantum computing, but it is fragile and can be easily destroyed by

the environment. The measure of entanglement including the operational methods to distinguish it from the separable case, however, is a tricky problem. So it is of practical significance to find a straightforward witnessing method. Here, we discuss efficiency of the new entropic uncertainty relation on witnessing entanglement in open quantum systems. We consider a system consists of two identical qubits which interact independently with their own reservoir, with the single “qubit+reservoir” Hamiltonian given by [18]

$$H = \omega_0 \sigma_+ \sigma_- + \sum_k \omega_k b_k^\dagger b_k + \sum_k (g_k b_k \sigma_+ + \text{h.c.}), \quad (9)$$

where ω_0 is the transition frequency of the qubit, and σ_\pm are the Pauli raising and lowering operators. The index k labels the reservoir field mode with frequency ω_k , with b_k^\dagger (b_k) being the bosonic creation (annihilation) operator and g_k being the coupling strength.

When the reservoir is at zero temperature and there is no correlation between the qubit and the reservoir initially, the single-qubit reduced density matrix $\rho^S(t)$ can then be determined as [18]

$$\rho^S(t) = \begin{pmatrix} \rho_{11}^S(0)|p(t)|^2 & \rho_{10}^S(0)p(t) \\ \rho_{01}^S(0)p^*(t) & 1 - \rho_{11}^S(0)|p(t)|^2 \end{pmatrix}, \quad (10)$$

where $\rho_{ij}^S(0) = \langle i | \rho^S(0) | j \rangle$ in the standard basis $\{|1\rangle, |0\rangle\}$, and the explicit time dependence of the single function $p(t)$ contains the information on the reservoir spectral density and the coupling constants.

After obtaining $\rho^S(t)$, the two-qubit density matrix $\rho(t)$ can then be determined by the procedure presented in [19]. Here we suppose the two qubits are prepared initially in the extended Werner-like (EWL) states [17]

$$\rho^\Xi(0) = r|\Xi\rangle\langle\Xi| + \frac{1-r}{4}\mathbb{I}, \quad (11)$$

where $|\Xi\rangle = |\psi\rangle$ or $|\phi\rangle$, with $|\psi\rangle = \alpha|00\rangle + e^{i\theta}\sqrt{1-\alpha^2}|11\rangle$ and $|\phi\rangle = \alpha|10\rangle + e^{i\theta}\sqrt{1-\alpha^2}|01\rangle$.

The density matrix $\rho^\Xi(t)$ depends only on the chosen initial state $\rho^\Xi(0)$ and values of the function $p(t)$ associated with the Hamiltonian model of Eq. (9), regardless of the reservoir structure. Thus in the following we ignore temporarily the explicit form of $p(t)$ and consider only the dependence of the uncertainties on p . The results obtained here thus apply to all cases where the single-qubit dynamics has the form of Eq. (10).

To witness the smallest amount of entanglement [4, 7], we choose the two observables as $R = \sigma_1$ and $S = \sigma_3$ in the following discussion. This choice of measurement operators gives the maximal complementarity between R and S ; that is, $c = 1/2$ and thus $\log_2(1/c) = 1$.

Consider first the initial state $\rho^\psi(0)$, for which the nonzero elements of $\rho^\psi(t)$ can be expressed in terms of $|p|^2$ (the diagonal elements) or p^2 (the antidiagonal elements) [19, 20]. Then one can check directly that uncertainty of the TE, BB as well as the concurrence (a

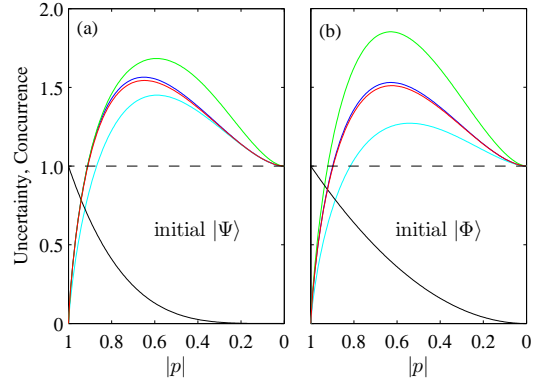


FIG. 2: (Color online) The $|p|$ dependence of FE, ME, TE, BB (from top to bottom) and concurrence (the bottommost) for the initial $|\Psi\rangle$ and $|\Phi\rangle$. The lines for FE and ME in panel (a) are plotted by choosing $p \in \mathbb{R}$.

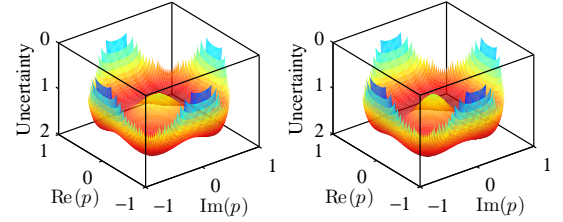


FIG. 3: (Color online) Dependence of the ME (left) and FE (right) on the real and imaginary parts of p for the initial $|\Psi\rangle$.

measure of entanglement) [21] are determined only by $|p|^2$ (they are also independent of θ), while the other two estimates (i.e., ME and FE) are determined by p^2 .

In Fig. 2(a) we plot the uncertainties versus $|p|$ (the ME and FE are plotted only with $p \in \mathbb{R}$), while in Fig. 3 we plot uncertainties of the ME and FE versus the real and imaginary parts of p , both for the initial state $|\Psi\rangle = (|00\rangle + |11\rangle)/\sqrt{2}$. Clearly, when $|p|$ is larger than a critical value $|p|_c$, the entanglement can always be witnessed by TE, and the related entanglement region does not explicitly depend on the particular choice of the reservoir. $|p|_c$ depends on the chosen initial state $\rho^\psi(0)$, and for $|\Psi\rangle$ it is of about 0.9101, which gives the entanglement region witnessed by it as $C^T \in [0.6858, 1]$.

From Fig. 3 one can see that the ME and FE are determined, however, by both $\text{Re}(p)$ and $\text{Im}(p)$, for there are p_1 and p_2 (those with the same distance to the origin of the coordinates) with $|p_1| = |p_2|$ but the uncertainties $U^{(M,F)}(p_1) < 1$ and $U^{(M,F)}(p_2) > 1$ (here $U^{(M,F)}$ represents uncertainties estimated by ME and FE). This means that, for this case, the entanglement regions witnessed by them are determined by the explicit structures of the reservoir and the coupling constant between the system and the reservoir. Of course, if $p \in \mathbb{R}$ we still have the entanglement regions depending only on $|p|$, and for the initial $|\Psi\rangle$ we obtained numerically $|p|_c \simeq 0.9116$, $C^M \in [0.6905, 1]$ for the ME, and

$|p|_c \simeq 0.9121$, $C^F \in [0.6921, 1]$ for the FE.

For the initial $\rho^\phi(0)$, the density matrix $\rho^\phi(t)$ is determined only by $|p|^2$, therefore all the uncertainty estimates as well as the entanglement regions witnessed by them are also determined by $|p|^2$, and thus are independent of the explicit structure of the reservoir. In Fig. 2(b) we give an exemplified plot of the $|p|$ dependence of different estimates for the initial state $|\Phi\rangle = (|10\rangle + |01\rangle)/\sqrt{2}$, for which we have $|p|_c \simeq 0.8962$, $C^T \in [0.8031, 1]$ for the TE, $|p|_c \simeq 0.8982$, $C^M \in [0.8068, 1]$ for the ME, and $|p|_c \simeq 0.8982$, $C^F \in [0.8486, 1]$ for the FE.

In the following we give some explicit examples of the structured reservoir to deepen our understanding of the above general arguments.

A. The sub-Ohmic, Ohmic and super-Ohmic reservoirs

We consider first the structured reservoirs with spectral densities of the form [22]

$$J(\omega) = \eta \omega^s \omega_c^{1-s} e^{-\omega/\omega_c}, \quad (12)$$

with η and ω_c being the dimensionless coupling constant and the cutoff frequency, which are related to the reservoir correlation time τ_B and the relaxation time τ_R (over which the state of the system changes in the Markovian limit of flat spectrum) by $\tau_B \approx \omega_c^{-1}$ and $\tau_R \approx \eta^{-1}$. Depending on the value of s , the reservoir is classified as sub-Ohmic if $0 < s < 1$, Ohmic if $s = 1$, and super-Ohmic if $s > 1$.

For this kind of reservoir spectral densities, $p(t)$ is determined by [23]

$$\dot{p}(t) + i\omega_0 p(t) + \int_0^t p(t_1) f(t-t_1) dt_1 = 0, \quad (13)$$

where the kernel function $f(t-t_1) = \int d\omega J(\omega) e^{-i\omega(t-t_1)}$ in the continuum limit the spectral density.

In this work we take $s = 1/2, 1$ and 3 as three examples of the sub-Ohmic, Ohmic, and super-Ohmic spectral densities. The kernel function can be integrated as $f(x) = \eta s! \omega_c^2 / (1 + i\omega_c x)^{s+1}$ ($x = t - t_1$) for $s \in \mathbb{Z}$, and $f(x) = \eta \omega_c^2 \sqrt{\pi} e^{-i\varpi} / [2(1 + \omega_c^2 x^2)^{3/4}]$ for $s = 1/2$, where $s!$ denotes the factorial of s , and $\varpi = \frac{3}{2} \tan^{-1}(\omega_c x)$. Then $p(t)$ can be solved numerically and the two-qubit density matrix can be derived by the procedure of [19].

In Fig. 4 we presented theoretical predictions of entanglement witness for the initial $|\Psi\rangle$ and $|\Phi\rangle$ in sub-Ohmic, Ohmic and super-Ohmic reservoirs, with $\eta = 0.01$ and $\omega_c = 2\omega_0$. One can see that while the concurrence decays monotonically and disappears in the infinite time limit, the different uncertainty estimates become larger than 1 after finite timescales. Thus there are critical $\omega_0 t_c$ after which the entanglement cannot be witnessed by them. For the TE, although the time interval $\omega_0 t_c$ is different for different spectral densities of the reservoirs and different system-reservoir coupling constants,

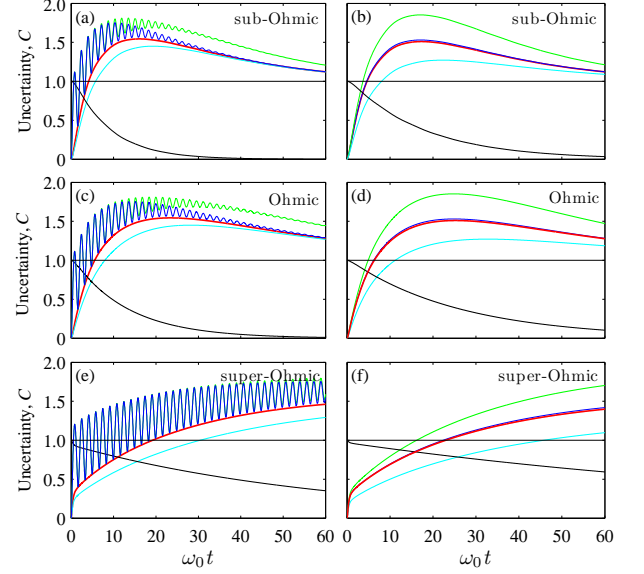


FIG. 4: (Color online) Entanglement witness in the sub-Ohmic, Ohmic and super-Ohmic reservoirs for the initial $|\Psi\rangle$ (left) and $|\Phi\rangle$ (right), with $\eta = 0.01$, $\omega_c = 2\omega_0$. The green, blue, red, cyan and black lines from top to bottom represent FE, ME, TE, BB, and the concurrence, respectively.

the numerical results confirm that the entanglement regions witnessed by it agree with those predicted in the general arguments (i.e., $C^T \in [0.6858, 1]$ for the initial $|\Psi\rangle$, and $C^T \in [0.8031, 1]$ for the initial $|\Phi\rangle$).

For the ME and FE, the regions of entanglement being witnessed will shrink, particularly, for the initial $|\Psi\rangle$, both the ME and FE oscillate around 1 with increasing $\omega_0 t$ in the short-time region (during which they are nearly overlapped), and the entanglement regions witnessed by them are discontinuous because here $p(t) \in \mathbb{C}$. For example, for parameters of Fig. 4(a) the discrete entanglement regions are $C^M \approx C^F \in [0.7501, 0.7897]$, $[0.8748, 0.9491]$ and $[0.9794, 1]$; that is, some states with a small amount of entanglement can be witnessed, while some others with a relatively large amount of entanglement cannot be witnessed. This reveals a counterintuitive fact; that is, not the more the state is entangled, the easier it can be witnessed for some schemes. For the initial $|\Phi\rangle$, the related entanglement regions are in accord with those predicted in the above general arguments, which are independent of the explicit time dependence of $p(t)$.

We also examined effects of the cutoff frequency ω_c on entanglement witness (for concise presentation in the paper, we did not plot them here), and found that for the sub-Ohmic and Ohmic spectral densities, $\omega_0 t_c$ decreases with increasing ω_c and their dependence on ω_c are weak ($\omega_0 t_c$ for $|\Phi\rangle$ is only a slightly larger than that for $|\Psi\rangle$). But for the super-Ohmic spectral density, $\omega_0 t_c$ is strongly dependent on ω_c ; for example, for the parameters of Figs. 4(e) and 4(f), they increase dramatically from 8.125 and 9.55 for $\omega_c = \omega_0$ to 165.525 and 196.85 for $\omega_c = 6\omega_0$.

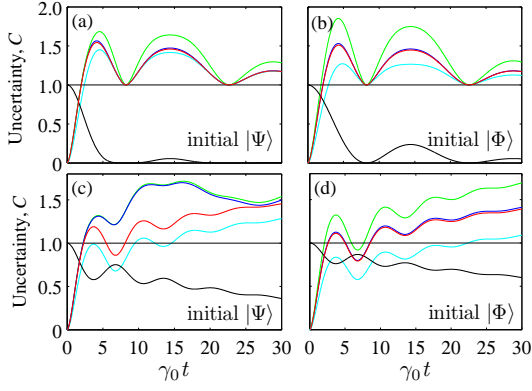


FIG. 5: (Color online) Entanglement witness in Lorentzian reservoir with the initial states $|\Psi\rangle$ and $|\Phi\rangle$, where $\lambda = 0.1\gamma_0$, $\delta = 0$ for panels (a) and (b), $\delta = 0.8\gamma_0$ for panels (c) and (d). The green, blue, red, cyan and black lines from top to bottom represent FE, ME, TE, BB, and the concurrence, respectively.

B. The Lorentzian reservoir

As the second example, we consider the structured reservoir with the Lorentzian spectral density [18]

$$J(\omega) = \frac{1}{2\pi} \frac{\gamma_0 \lambda^2}{(\omega - \omega_c)^2 + \lambda^2}, \quad (14)$$

where λ denotes the spectral width of the reservoir and is related to the reservoir correlation time via $\tau_B \approx \lambda^{-1}$, and γ_0 is related to the relaxation time τ_R via $\tau_R \approx \gamma_0^{-1}$. $\lambda > 2\gamma_0$ ($\lambda < 2\gamma_0$) corresponds to the Markovian (non-Markovian) regime, and $\omega_c = \omega_0 - \delta$ is the central frequency of the reservoir detuned from the transition frequency ω_0 by an amount δ .

The function $p(t)$ can be derived analytically as [24]

$$p(t) = e^{-\frac{1}{2}(\lambda - i\delta)t} \left[\cosh \frac{dt}{2} + \frac{\lambda - i\delta}{d} \sinh \frac{dt}{2} \right], \quad (15)$$

with $d = [(\lambda - i\delta)^2 - 2\gamma_0\lambda]^{1/2}$. Thus the two-qubit density matrix can also be derived analytically [19].

To explore efficiency of entanglement witness for this kind of system-reservoir coupling, we plot in Fig. 5 theoretical predictions of uncertainties in the non-Markovian regime ($\lambda = 0.1\gamma_0$) with the initial $|\Psi\rangle$ and $|\Phi\rangle$. Clearly, they oscillate with increasing $\gamma_0 t$, and the time regions during which the entanglement can be witnessed depend on δ and λ . But in the absence of detuning (i.e., $\delta = 0$), the numerical results show that the entanglement regions witnessed by different estimates are independent of λ , and are consistent with those predicted in the above general arguments, which can be understood from the fact that when $\delta = 0$ we always have $p(t) \in \mathbb{R}$.

Introducing detuning will decrease the decay rate of entanglement, and as can be seen from Figs. 5(c) and 5(d), the time regions during which the entanglement can be witnessed become discontinuous, even for the TE. But the entanglement regions witnessed by TE remains the

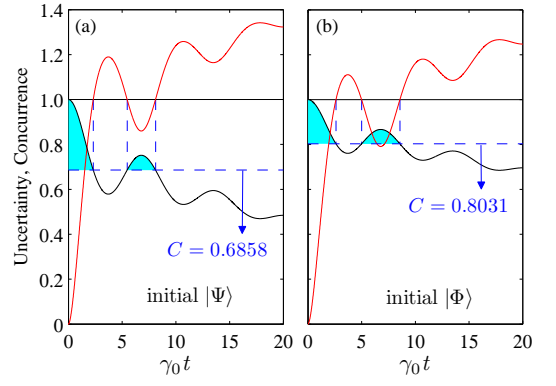


FIG. 6: (Color online) Comparison of the entanglement (black) witnessed by TE (red) at different time regions, where the two panels are plotted with completely the same parameters as those in Figs. 5(c) and 5(d), respectively.

same (see the green shaded regions in Fig. 6) as that for $\delta = 0$. Furthermore, for the initial $|\Psi\rangle$, the entanglement regions witnessed by ME and FE vary with the variation of λ (their dependence on λ may be very weak for certain parameters, e.g., $\delta = 0.8\gamma_0$ and $\lambda > 0.5\gamma_0$), which is caused by $p(t) \in \mathbb{C}$ when $\delta \neq 0$. For the initial $|\Phi\rangle$, they remain the same as those for $\delta = 0$, and do not depend on the parameter λ .

IV. SUMMARY

In summary, we have studied relations between the quantum-memory-assisted entropic uncertainty principle, teleportation and entanglement witness. We proved geometrically that any two-qubit state with negative conditional von Neumann entropy, which thus lowers down the upper bound of the entropic uncertainty relation, is useful for teleportation (i.e., $F_{av} > 2/3$). We have also examined efficiency of this new entropic uncertainty principle on witnessing entanglement in a general class of bosonic structured reservoirs, and found that the entanglement regions witnessed by TE for the initial EWL state $\rho^\psi(0)$ or that witnessed by all the three estimates TE, ME and FE for the initial EWL state $\rho^\phi(0)$ are determined only by a function p , which has no relation with the explicit form of its time dependence. These general arguments are corroborated by explicit examples of structured reservoirs with the sub-Ohmic, Ohmic, super-Ohmic and Lorentzian spectral densities. As a by-product, we also found that it is not a general result that the more the state is entangled, the easier it can be witnessed for certain chosen schemes.

As the quantum-memory-assisted entropic uncertainty principle has been experimentally realized [4, 9], and it is possible to simulate and control the Markovian and non-Markovian environments [25–27], we expect the results demonstrated in this work may be certified in future experiments with currently available technologies;

for example, by using two-level atoms confined in optical microcavities [28] or simulated reservoirs [29].

ACKNOWLEDGMENTS

This work was supported by NSFC (11205121,

10974247, 11175248), “973” program (2010CB922904), NSF of Shaanxi Province (2010JM1011), and the Scientific Research Program of Education Department of Shaanxi Provincial Government (12JK0986).

-
- [1] W. Heisenberg, Z. Phys. **43**, 172 (1927).
 - [2] H. P. Robertson, Phys. Rev. **34**, 163 (1929).
 - [3] C. H. Bennett and G. Brassard, in *Proceedings of the IEEE International Conference on Computers, Systems and Signal Processing* (Bangalore, India, 1984), pp. 175-179; M. Tomamichel, C. C. W. Lim, N. Gisin, and R. Renner, Nature Commun. **3**, 634 (2012).
 - [4] R. Prevedel, D. R. Hamel, R. Colbeck, K. Fisher, and K. J. Resch, Nature Phys. **7**, 757 (2011).
 - [5] I. Białynicki-Birula and J. Mycielski, Commun. Math. Phys. **44**, 129 (1975); D. Deutsch, Phys. Rev. Lett. **50**, 631 (1983); K. Kraus, Phys. Rev. D **35**, 3070 (1987); H. Maassen and J. B. M. Uffink, Phys. Rev. Lett. **60**, 1103 (1988).
 - [6] J. M. Renes and J. C. Boileau, Phys. Rev. Lett. **103**, 020402 (2009).
 - [7] M. Berta, M. Christandl, R. Colbeck, J. M. Renes, and R. Renner, Nature Phys. **6**, 659 (2010).
 - [8] N. J. Cerf and C. Adami, Phys. Rev. Lett. **79**, 5194 (1997); I. Devetak and A. Winter, Proc. R. Soc. A **461**, 207 (2005).
 - [9] C. F. Li, J. S. Xu, X. Y. Xu, K. Li, and G. C. Guo, Nature Phys. **7**, 752 (2011).
 - [10] M. Tomamichel and R. Renner, Phys. Rev. Lett. **106**, 110506 (2011); Z. Y. Xu, W. L. Yang, and M. Feng, Phys. Rev. A **86**, 012113 (2012); P. J. Coles, e-print arXiv:1203.3153; A. K. Pati, A. R. Usha Devi, A. K. Rajagopal, and Sudha, e-print arXiv:1204.3803.
 - [11] C. H. Bennett, G. Brassard, C. Crépeau, R. Jozsa, A. Peres, and W. K. Wootters, Phys. Rev. Lett. **70**, 1895 (1993).
 - [12] A. Osterloh, L. Amico, G. Falci and R. Fazio, Nature **416**, 608 (2002).
 - [13] J. Cui, M. Gu, L. C. Kwek, M. F. Santos, H. Fan, and V. Vedral, Nature Commun. **3**, 812 (2012).
 - [14] M. A. Nielsen and I. L. Chuang, *Quantum Computation and Quantum Information* (Cambridge University Press, Cambridge, UK, 2000).
 - [15] R. Horodecki, M. Horodecki, and P. Horodecki, Phys. Lett. A **222**, 21 (1996).
 - [16] R. Horodecki and M. Horodecki, Phys. Rev. A **54**, 1838 (1996).
 - [17] R. F. Werner, Phys. Rev. A **40**, 4277 (1989); B. Bellomo, R. Lo Franco, and G. Compagno, *ibid.* **77**, 032342 (2008).
 - [18] H.-P. Breuer and F. Petruccione, *The Theory of Open Quantum Systems* (Oxford University Press, Oxford, 2002).
 - [19] B. Bellomo, R. Lo Franco, and G. Compagno, Phys. Rev. Lett. **99**, 160502 (2007).
 - [20] B. Bellomo, R. Lo Franco, S. Maniscalco, and G. Compagno, Phys. Rev. A **78**, 060302 (2008).
 - [21] W. K. Wootters, Phys. Rev. Lett. **80**, 2245 (1998).
 - [22] A. J. Leggett, S. Chakravarty, A. T. Dorsey, M. P. A. Fisher, A. Garg, and W. Zwerger, Rev. Mod. Phys. **59**, 1 (1987).
 - [23] Q. J. Tong, J. H. An, H. G. Luo, and C. H. Oh, J. Phys. B **43**, 155501 (2010).
 - [24] M. L. Hu and H. Fan, Ann. Phys. **327**, 2343 (2012).
 - [25] M. P. Almeida, F. de Melo, M. Hor-Meyll, A. Salles, S. P. Walborn, P. H. Souto Ribeiro, and L. Davidovich, Science **316**, 579 (2007).
 - [26] J. S. Xu, X. Y. Xu, C. F. Li, C. J. Zhang, X. B. Zou, and G. C. Guo, Nature Commun. **1**, 7 (2010).
 - [27] B. H. Liu, Y. F. Huang, C. F. Li, G. C. Guo, E. M. Laine, H. P. Breuer, and J. Piilo, Nature Phys. **7**, 931 (2011).
 - [28] K. J. Vahala, Nature **424**, 839 (2003).
 - [29] I. Buluta and F. Nori, Science **326**, 108 (2009); D. Porras, F. Marquardt, J. von Delft, and J. I. Cirac, Phys. Rev. A **78**, 010101 (2008).